Fifth International Conference on CFD in the Process Industries
CSIRO, Melbourne, Australia
13-15 December 2006

MODELLING OF COLD METAL EXTRUSION USING SPH

Mahesh PRAKASH and Paul W. CLEARY
[1]CSIRO Mathematical and Information Sciences, Clayton, VIC 3169

ABSTRACT

Extrusion is often used for producing long objects with constant cross-sections. The process is used with both hot and cold metal and also plastics. Extrusion modelling can be used to reduce trial extrusion numbers because of better process design following from accurate defect prediction. Such models can also be used as input for die-design activities and to indicate ways for improving non-performing dies.

Traditionally, the extrusion process has been modelled using mesh based Finite Element Methods (FEM). However, the large plastic deformations occurring in the billets during extrusion can often lead to heavy re-meshing requirements for such methods and excessive numerical diffusion. Here we demonstrate the use of the mesh-less Smoothed Particle Hydrodynamics (SPH) method for simulating such processes. Its grid-free nature allows SPH to handle large deformations without the need for any re-meshing. Additionally SPH provides the ability to track history dependent properties such as plastic strain on a particle by particle basis making it very suitable for analysis and defect prediction.

In this paper we evaluate the variation in plastic strain level and deformation profile in a typical aluminium alloy with extrusion parameters such as die diameter and die angle. We also investigate the effect of these parameters on the maximum extrusion force required.

INTRODUCTION

Extrusion can be defined as the production of a part of a desired shape by forcing a solid metal billet to flow through a die. Extrusion is often used in making automotive and building hardware parts where high strength and close tolerances are required. The advantages of modelling extrusion include:

- Ability to verify empirical knowledge
- Reduction of trial-pressings
- Usability in input for die design programs
- Indication of methods to improve non-functional dies.

Large plastic deformations in the metal during extrusion can lead to heavy re-meshing requirements for FEM methods (Tiernan et al. 2005) which can be inaccurate and diffusive. Due its mesh-free nature such large deformations can be easily handled by SPH (Fernandez-Mendez et al. 2005). The particle based nature of the method also gives it the ability to track history dependent properties such as surface oxide formation and plastic strain on a node by node basis even during very large deformations, Cleary et al. (2006).

Here we evaluate, for a simple 3D cold extruded part:

- Variation in plastic strain levels,
- Variation in metal deformation patterns and
- Variation in maximum extrusion force required;

with changes in extrusion parameters such as die diameter and die angle.

THE SPH METHOD

A brief summary of the SPH method is presented here. For more comprehensive details one can refer to Gray et al., 2001. The interpolated value of a function A at any position $\mathbf{r}$ can be expressed using SPH smoothing as:

$$A(\mathbf{r}) = \sum_b m_b \frac{A_b}{\rho_b} W(\mathbf{r} - \mathbf{r}_b, h) \tag{1}$$

where m_b and $\mathbf{r}_b$ are the mass and density of particle b and the sum is over all particles b within a radius 2h of $\mathbf{r}$. Here $W(\mathbf{r},h)$ is a C^2 spline based interpolation or smoothing kernel with radius 2h, that approximates the shape of a Gaussian function but has compact support. The gradient of the function A is given by differentiating the interpolation equation (1) to give:

$$\nabla A(\mathbf{r}) = \sum_b m_b \frac{A_b}{\rho_b} \nabla W(\mathbf{r} - \mathbf{r}_b, h) \tag{2}$$

Using these interpolation formulae and suitable finite difference approximations for second order derivatives, one is able to convert parabolic partial differential equations into ordinary differential equations for the motion of the particles and the rates of change of their properties.

Continuity Equation

From Monaghan (1992), our preferred form of the SPH continuity equation is:

$$\frac{d\rho_a}{dt} = \sum_b m_b (\mathbf{v}_a - \mathbf{v}_b) \bullet \nabla W_{ab} \tag{3}$$

where ρ_a is the density of particle a with velocity $\mathbf{v}_a$ and m_b is the mass of particle b. We denote the position vector from particle b to particle a by $\mathbf{r}_{ab} = \mathbf{r}_a - \mathbf{r}_b$ and let $W_{ab} = W(\mathbf{r}_{ab}, h)$ be the interpolation kernel with smoothing length h evaluated for the distance $|\mathbf{r}_{ab}|$. This form of the continuity equation is Galilean invariant (since the positions and velocities appear only as differences), has good numerical conservation properties and is not affected by free surfaces or density discontinuities.

Momentum Equation

The momentum equation used for the elasto-plastic deformation of the solids is:

$$\frac{dv^i}{dt} = \frac{1}{\rho_s} \frac{\partial \sigma^{ij}}{\partial x^j} + g^i \ , \tag{4}$$

where v is velocity, g denotes the body force and σ is the stress tensor which can be written as:

$$\sigma^{ij} = -P_s \delta^{ij} + S^{ij} \ , \tag{5}$$

where P_s is the pressure and S is the deviatoric stress. Assuming Hooke's law with shear modulus μ_s the evolution equation for the deviatoric stress S is (Gray et al., 2001):

$$\frac{dS^{ij}}{dt} = 2\mu_s\left(\dot{\varepsilon}^{ij} - \frac{1}{3}\delta^{ij}\dot{\varepsilon}^{ij}\right) + S^{ik}\Omega^{jk} + \Omega^{ik}S^{kj} \qquad (6)$$

where

$$\dot{\varepsilon}^{ij} = \frac{1}{2}\left(\frac{\partial v^i}{\partial x^j} + \frac{\partial v^j}{\partial x^i}\right) \qquad (7)$$

and

$$\Omega^{ij} = \frac{1}{2}\left(\frac{\partial v^i}{\partial x^j} - \frac{\partial v^j}{\partial x^i}\right) \qquad (8)$$

is the rotation tensor.

The subscript s in the above symbols refers to the solid state. The bulk modulus is $K = \overline{\rho}_s c_0^2$ and the Poisson ratio ν_s is:

$$\nu_s = \frac{(3K/\mu_s - 2)}{2(3K/\mu_s + 2)} \qquad (9)$$

Equation of State

The SPH method used here is quasi-compressible with the pressure calculated from the particle density using an equation of state:

$$P_{s0} = c_0^2(\rho_s - \rho_{s0}) \qquad (10)$$

where Ps_0 is the magnitude of the pressure and ρ_0 is the reference density. The pressure scale factor Ps_0 is given by:

$$\frac{\gamma P_{s0}}{\rho_0} = 100V^2 = c_s^2 \qquad (11)$$

where V is the characteristic or maximum velocity. This ensures that the density variation is less than 1% and the material can be regarded as incompressible.

Plasticity Model

The plasticity model used is a radial return plasticity model originally proposed by Wilkins (1964). The trial stress S_{Tr}^{ij} is the deviatoric part of the stress calculated assuming that the initial response is elastic,

$$S^{ij} = \alpha S_{Tr}^{ij} \qquad (12)$$

where S^{ij} is the final deviatoric stress at the end of a time-step and α is a proportionality constant given by:

$$\alpha = \left(1 - \frac{3\mu_s \Delta\bar{\varepsilon}^p}{\bar{\sigma}^{Tr}}\right) \qquad (13)$$

with $\sqrt{2/3}\,\bar{\sigma}^{Tr}$ being the magnitude of the trial deviatoric stress and $\Delta\bar{\varepsilon}^p$ being the increment in equivalent plastic strain:

$$\Delta\bar{\varepsilon}^p = \frac{\bar{\sigma}^{Tr} - \sigma_y^n}{3\mu_s + H} \qquad (14)$$

where σ_y^n is the final yield stress and H is the hardening modulus. The stress update is completed by adding the deviatoric and mean stress as given in equation (5). The plastic strain is incremented as:

$$\bar{\varepsilon}^p = \bar{\varepsilon}^p + \Delta\bar{\varepsilon}^p \qquad (15)$$

History Dependent Properties of the Metal

Each SPH particle represents a specific volume of metal and carries that information with it. This is a critical attribute of the Lagrangian methods. This means that information on the precise state of each piece of metal can be known at all times and the history of each piece of metal is built into the particle data. This provides significant capability to track properties such as:

- Cumulative plastic strain
- Damage (which is a volume averaged local measure of cracking) leading to fracture prediction;
- Metal composition (including tracking multiple metals or metal composites) and trapped gas;
- Metallic phase and microstructure; and
- Surface oxide.

Some or all of these properties can then be used to feed back into the flow dynamics using suitable rheology models.

EXTRUSION MODELLING USING SPH

Figure 1 shows a front view of the extrusion geometry consisting of a 3D cylindrical billet of diameter D = 40 mm, which is cold extruded through a die exit diameter d = 20, 15 or 10 mm with a punch moving at a constant speed of 25 m/min. Die angles of θ = 120, 140 or 160 degrees were used for the simulations. The material properties of the aluminium alloy are presented in Table 1. An SPH particle resolution of 1.6 mm was used giving a total of 7,760 particles for these three dimensional simulations.

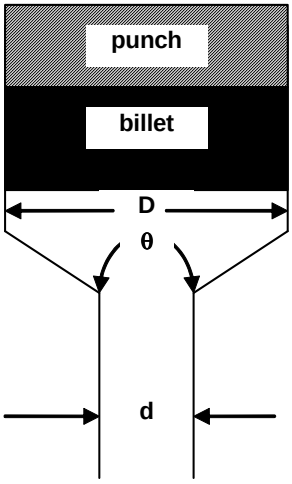

Figure 1: Schematic diagram of extrusion geometry.

In cold extrusion modelling it is common to use a rigid-plastic model to describe the material behaviour (Tiernan et al., 2005). However in certain circumstances elastic effects can become important especially in a cylindrical channel where elastic effects can have a significant impact on the results (Lof, 2000). In this paper the elasto-plastic model described earlier is used to represent the alloy behaviour.

Effect of die diameter on plastic strain and deformation

The effect of die diameter on plastic strain and internal billet deformation is demonstrated using three cases with a constant die angle of 120° and varying die exit diameters of 20, 15 and 10 mm.

Bulk Modulus (GPa)	7.0
Shear Modulus (GPa)	2.70
Initial Yield Stress (MPa)	5.52
Hardening Modulus (MPa)	0.0
Density (kg/m^3)	2700.0

Table 1: Properties of Al alloy used for cold extrusion.

Figure 2 shows the billet coloured by percentage plastic strain with blue being minimum and red showing maximum strain level fixed at 2.1 or 210% percent for all three cases. Figure 3 shows metal deformation profiles for the three exit diameters. In Figure 3 the billet is coloured in horizontal strata based on initial material position in order to track the internal metal deformation profile. A section view of the 3D billet is shown in this figure.

At 20 ms the billet has not yet moved into the die exit for the d = 20 mm case since a large amount of metal needs to be pushed through the die for the larger exit diameter. Plastic strain levels are very low for this case at this stage. For d = 15 mm, the metal has moved into the die exit with approximately a quarter of the billet experiencing a low to moderate amount of strain. Once the billet corners contact the converging walls of the die, the metal is quickly elastically loaded and begins undergoing plastic deformation. For d =10 mm, a reasonable amount of metal has been already been extruded through the die at 20 ms with the metal experiencing high strain levels in excess of 210% as it passes through the relatively small die orifice.

At 30 ms the metal has progressed into the die for d = 20 mm case with high strain levels developing in regions adjacent to the die walls. For d = 15 mm, significant amounts of metal have passed through the die orifice and have experienced strain levels greater than 210%. The central material at the leading surface has a lower strain. For d = 10 mm, the amount of high strain is very large with almost the entire extruded metal length now experiencing strain levels greater than 210% including the central region. This indicates that for large extrude ratios (ratio of billet diameter to product diameter) strain levels can be significantly high throughout the extruded product and not just regions adjacent to the walls. Products with large extrude ratios will thus have a higher tendency to fail in the absence of a rigorous annealing process after cold extrusion (Shivpuri et al., 1999).

By 40 ms, significant amounts of extruded product have been produced for all three die diameters. For d = 20 mm, the high plastic strain levels adjacent to the walls have now become more pronounced. The central region (except at the leading edge) also develops medium amounts of strain of around 160%. A second low strain cell starts to develop in the central core at this time. For d = 15 mm, high strain levels of around 210% are now seen even in the central region away from the leading edge. Here again there are pockets or cells of medium strain levels in the core coloured yellow although the size of these cells are much smaller in comparison to the d = 20 mm case. Such pockets are developed since the two high plastic strain regions from the two walls do not meet completely and could lead to a defect referred to as chevron crack (Saanouni K. et al., 2004). The occurrence of such pockets can be reduced by increasing the extrusion ratio (as seen from the d = 10 mm case).

By 70 ms, the central low strain cell is clearly seen for the d = 20 mm case as the billet is almost fully extruded through the die. As the end of the billet approaches the convergent section a clear strain concentration occurs in the central core. For d = 15 mm, the central cells are more stretched and less pronounced. For d = 10 mm the metal passes through the die with high strain levels throughout the metal mass. The simulations show that even at very high extrusion ratios leading to large deformations no special treatment is required with the SPH methodology.

Effect of die angle on plastic strain and deformation

The effect of die angle on plastic strain and internal billet deformation is demonstrated using three cases with a constant die diameter of 20 mm and varying die angles of 120, 140 and 160^o. Figure 4 shows the billet coloured by percentage plastic strain with blue being minimum and red showing maximum strain level fixed at 2.1 or 210% percent for all three cases. Figure 5 shows metal deformation profile as in the previous section.

At 20 ms, the metal has just moved into the die opening for the 120^o case with the metal not yet reaching the die for the higher die angles due to larger volumes needing to be filled before reaching the die entrance. The metal at the leading edge has assumed the shape of the die entrance for the 120° case. For the larger die angles the metal front is still fairly flat at this stage.

At 30 ms, the metal has moved into the die for all three cases with more metal already being extruded for the smaller die angle. The metal deformation profiles for the three cases are quite similar with the only difference being a delay in the metal extrusion with increasing die angle. For the 120° case the metal deformation profile has a v-shaped structure at this stage as seen from the green coloured band.

At 40 ms increased strain levels can be seen at regions adjacent to the die walls for all three die angles. Note that in these simulations frictional effects have not been taken into consideration with normal forces accounting for high strain levels. The metal deformation profile for all three angles reveal a parabolic pattern at the leading edge at this stage.

At 50 ms the effect of normal force leading to high strain regions becomes more prominent. This is seen most clearly with a die angle of 160° where the die walls at the entrance are almost orthogonal to the metal entering the die.

At 74 ms, the metal has almost completely extruded through the die for all three cases. A central cell with metal at a low strain level (coloured green) is seen for all three cases. Except for a relatively higher strain level adjacent to the side walls for the 160^o angle case the strain levels and metal deformation profiles for all three cases are similar. This indicates that the die angle has little impact on the quality or properties of the extrusion.

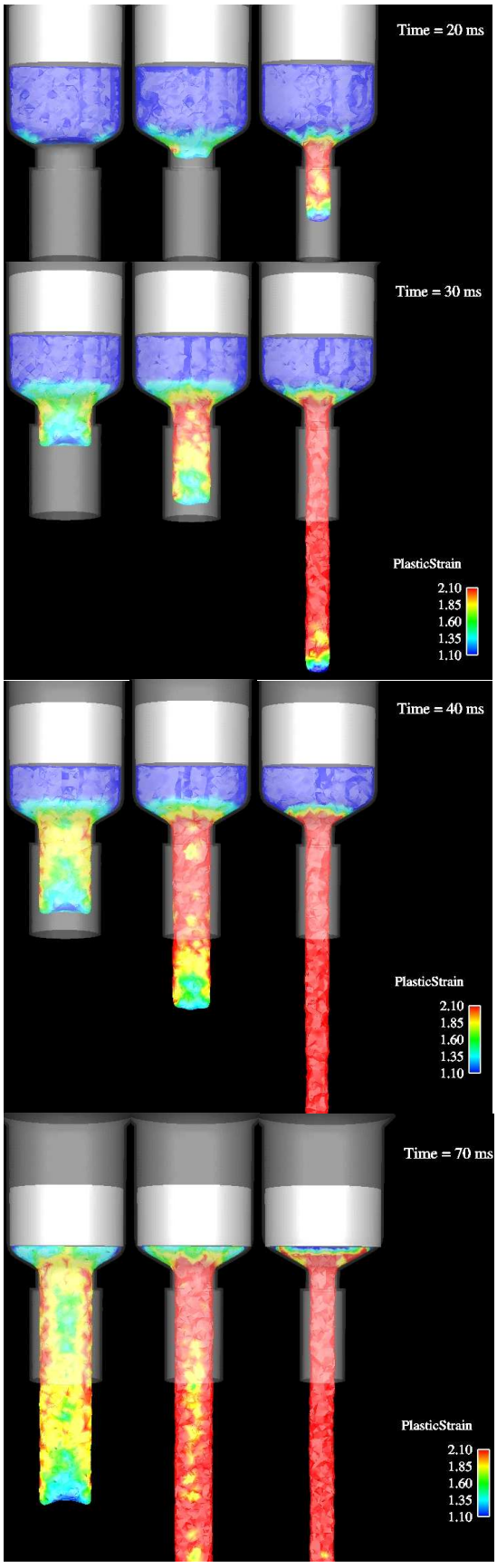

(a) (b) (c)

Figure 2: Plastic strain increases strongly with a decrease in die diameter (a) 20 mm (b) 15 mm (c) 10 mm.

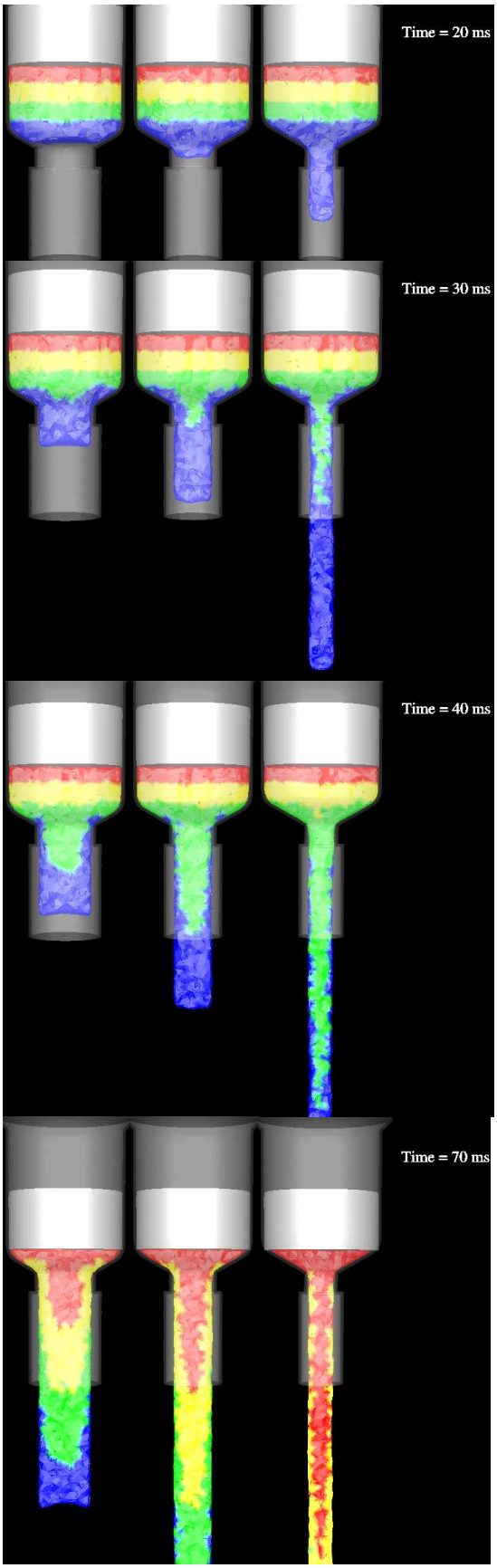

(a) (b) (c)

Figure 3: The extent of metal deformation increases with decrease in die diameter (a) 20 mm (b) 15 mm (c) 10 mm.

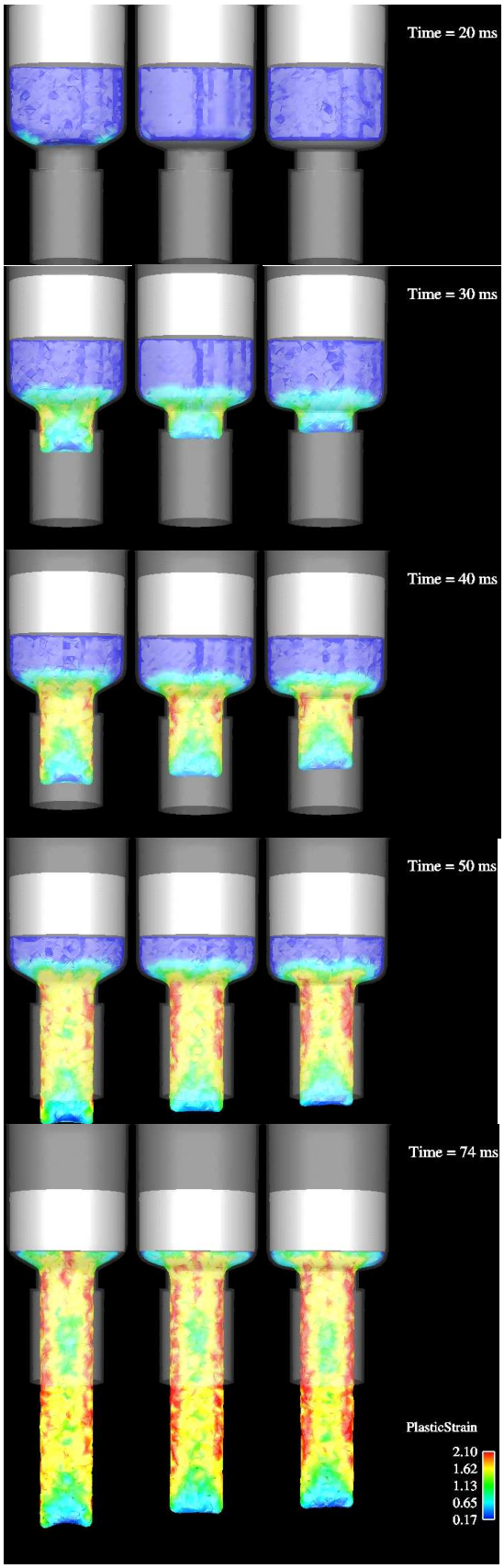

(a) (b) (c)

Figure 4: Plastic strain increases with increase in die angle (a) 120 deg (b) 140 deg (c) 160 deg.

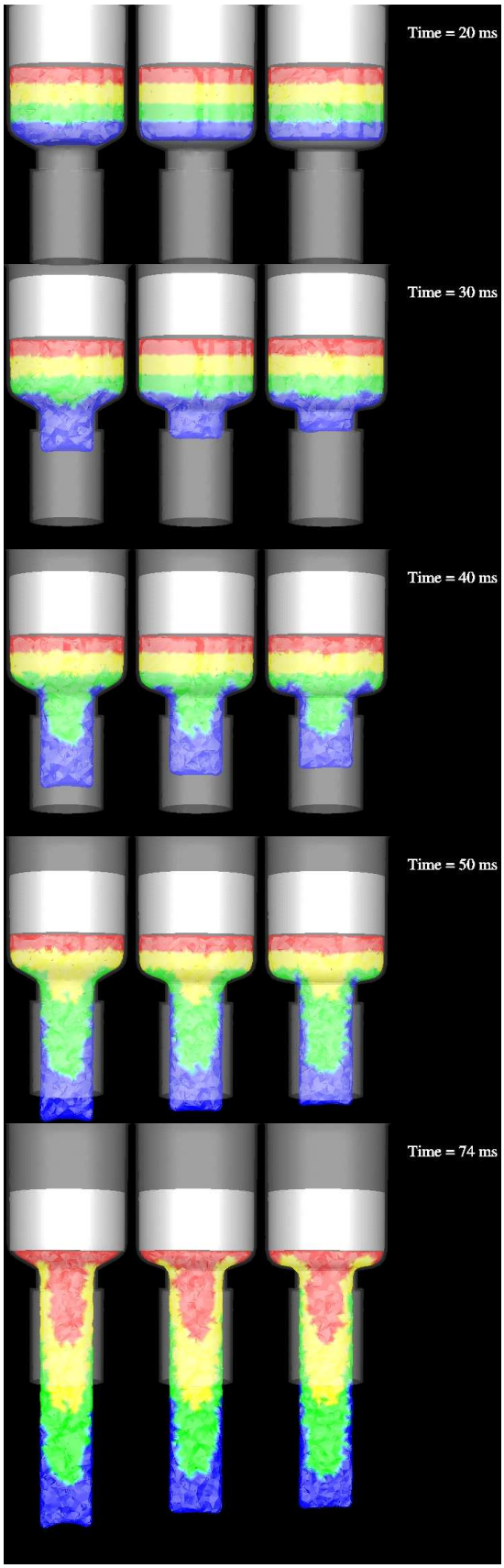

(a) (b) (c)

Figure 5: Metal deformation does not change significantly with die angle (a) 120 deg (b) 140 deg (c) 160 deg.

Effect of die diameter and angle on extrusion force

Figure 6 shows the effect of die diameter on the extrusion force required. The extrusion force ramps up over the first 15-20 ms to a maximum value as the billet fills the region around the die inlet. Between 20 and 60 ms, the metal is extruded at a constant rate through the die giving a consistent force at around the maximum level. The force then oscillates as the rear of the billet approaches the extrusion region and then declines rapidly. As shown in Table 2 the extrusion force increases with an increase in the extrusion ratio with the d = 10 mm case experiencing the maximum force of 30 kN which is around 150% greater than the d = 20 mm case. This result is qualitatively consistent with results obtained from previous studies of a similar nature using the finite element method (Tiernan et al., 2005).

Case	Die exit diameter (mm)	Die angle (degrees)	Maximum force (kN)
1	20	120	12
2	15	120	17
3	10	120	30
4	20	140	13
5	20	160	14

Table 2: Maximum extrusion force with variation in die diameter and angle.

Figure 7 shows the effect of die angle on the extrusion force. Again the extrusion force ramps up to its maximum value by around 20 ms for all three cases. It increases moderately with die angle, with the variation between the three cases being around 15% as seen from the maximum force values in Table 2.

With an increase in die angle there is evidence of strong oscillations in the extrusion force with an almost periodic behaviour. For the 160° case the oscillations have an amplitude of approximately 2.4 kN and a frequency of around 125 Hz.

Due to the absence of frictional effects we see an increase in the normal force required with an increase in the die angle. This will only be true in situations where a very good lubricant is used for the extrusion process such as in hydrostatic cold extrusion (Swiostek et al., 2006). However in many extrusion cases one will need to include frictional effects and this will alter the relationship between die angle and extrusion force required.

CONCLUSION

The SPH method can be effectively used for modelling metal extrusion processes using an elasto-plastic model for the metal rheology. For these metal forming processes, SPH has the advantages of being able to follow very high deformations (beyond what is possible with FEM and FV methods) and to keep track of the specific history of each part of the metal allowing fine scale control over the rheology model and potentially direct prediction of many types of flow and microstructure related defects.

Additionally the effect of changes in extrusion parameters such as extrusion ratio and die angle on plastic strain, metal deformation profile and maximum extrusion force required can effectively and easily be analysed using SPH. Specifically we have shown that:

- Plastic strain on the metal increases sharply with increasing extrusion ratio, with high plastic strains observed throughout the metal for large extrusion ratios.
- Plastic strain increases moderately with an increase in die angle especially in regions adjacent to the walls of the die.
- The maximum extrusion force increases sharply with an increase in extrusion ratio, with a variation of around 150% between extrusion ratios of 2:1 and 4:1..
- The maximum extrusion force shows only a small increase with die angle giving a variation of around 15% for the three die angles considered.

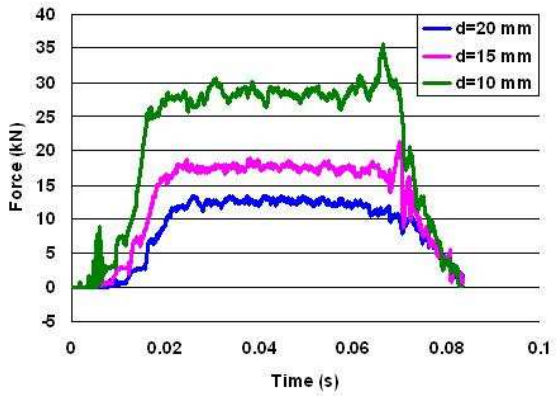

Figure 6: Extrusion force increases with decrease in die diameter (a) 20 mm (b) 15 mm (c) 10 mm.

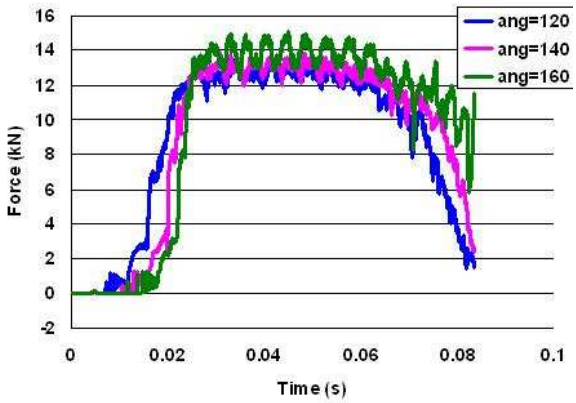

Figure 7: Extrusion force increases with increase in die angle (a) 140 deg (b) 160 deg (c) 180 deg. The present simulations assume perfect lubrication (no friction).

REFERENCES

CLEARY, P.W., PRAKASH, M., HA, J., STOKES, N., and SCOTT, C., (2005), "Smooth Particle Hydrodynamics; Status and future potential", *Proc. 4th Int. Conf. on CFD in the Oil and Gas, Metall. & Process Industries*, Norway, Eds. S.T. Johansen, I.G. Page.

FERNANDEZ-MENDEZ, S., BONET, J. HUERTA, A., (2005), "Continuous blending of SPH with finite elements", *Computers and Structures*, **83**, 1448-1458.

GRAY, J. P., MONAGHAN, J. J. and SWIFT, R. P., (2001), "SPH elastic dynamics", *Comput. Methods Appl. Mech. Engg.*, **190**, 6641-6662.

LOF, J., (2000), "Developments in finite element simulations of aluminium extrusion", *PhD Thesis*, University of Twente, Netherlands.

MONAGHAN, J. J., (1992), "Smoothed particle hydrodynamics", *Ann. Rev. Astron. Astrophys.*, **30**, 543-574.

SAANOUNI K., MARIAGE, J. F., CHEROUAT, A., LESTRIEZ, P., (2004), "Numerical prediction of discontinuous central bursting in axisymmetric forward extrusion by continuum damage mechanics", *Computers and Structures*, **82**, 2309-2332.

SHIVPURI, R., PABALKAR, A., SURIYANARAYANAN, K., KINI, S., (1999), "Formability issues in the cold extrusion of rolled rod", *Proc. 41st MWSP Conference, ISS, Vol. XXXVII*, 665-676.

SWIOSTEK, J., GOKEN, J., LETZIG, D. and KAINER, K. U., (2006), "Hydrostatic extrusion of commercial magnesium alloys at 100°C and its influence on grain refinement and mechanical properties", *Material Science and Engineering A*, **424**, 223-229.

TIERNAN, P., HILLERY, M. T., DRAGANSECU, B., GHEORGHE, M., (2005), "Modelling of cold extrusion with experimental variation", *Journal of Materials Processing Technology*, **168**, 360-366.

WILKINS, J.L., (1964), "Calculation of Elastic-plastic Flow", *Methods of Computational Physics*, Academic Press, New York, **8**.